Fabrication of ultrathin multilayered superomniphobic nanocoatings by liquid flame spray, atomic layer deposition and silanization

Miika Sorvali[1], Leena Vuori[2], Marko Pudas[3], Janne Haapanen[1], Riitta Mahlberg[4], Helena Ronkainen[4], Mari Honkanen[5], Mika Valden[2], Jyrki M. Mäkelä[1]

[1]Aerosol Physics, Laboratory of Physics, Faculty of Natural Sciences, Tampere University of Technology, P.O. Box 692, FI-33101 Tampere, Finland

[2]Surface Science, Laboratory of Photonics, Faculty of Natural Sciences, Tampere University of Technology, P.O. Box 692, FI-33101 Tampere, Finland

[3]Picosun Oy, FI-02430 Masala, Finland

[4]VTT Technical Research Center of Finland, P.O. Box 1000, FI-02044 Espoo, Finland

[5]Materials Characterization, Laboratory of Materials Science, Faculty of Engineering Sciences, Tampere University of Technology, P.O. Box 589, FI-33101 Tampere, Finland

ABSTRACT

Superomniphobic, i.e. liquid-repellent, surfaces have been an interesting area of research during the last decade due to their various potential applications. However, producing such surfaces, especially on hard and resilient substrates like stainless steel, still remains challenging. We present a stepwise fabrication process of a multilayered nanocoating on a stainless steel substrate, consisting of a nanoparticle layer, a nanofilm and a layer of silane molecules. Liquid flame spray (LFS) was used to deposit a TiO_2 nanoparticle layer on the bottom for producing a suitable surface structure. The interstitial Al_2O_3 nanofilm, fabricated by atomic layer deposition (ALD), stabilized the nanoparticle layer, and the topmost fluorosilane layer lowered the surface energy of the coating for enhanced omniphobicity. The coating was characterized with field emission scanning electron microscopy (FESEM), focused ion beam scanning electron microscopy (FIB-SEM), x-ray photoelectron spectroscopy (XPS), contact angle (CA) and sliding angle (SA) measurements, and microscratch testing. The widely recognized requirements for superrepellency, i.e. CA > 150° and SA < 10°, were achieved for deioinized water, diiodomethane and ethylene glycol. The mechanical stability of the coating could be varied by tuning the thickness of the ALD layer at the expense of repellency. To our knowledge, this is the thinnest superomniphobic coating reported so far, with the average thickness of about 70 nm.

INTRODUCTION

Since surfaces are often in contact with water or other liquids, controlling their wettability has been an interesting research area for several decades. A surface is considered hydrophobic if it forms with a water droplet a contact angle greater than 90° and superhydrophobic when this angle exceeds 150°. If this water-repellency is extended to also cover other liquids, the terms

superomniphobic and -amphiphobic are introduced. We will use the former in this paper, but the two are basically equivalent in meaning. True superrepellency also requires either the contact angle hysteresis, i.e. the difference between the advancing and receding contact angles, or the smallest inclination angle of the surface that makes the droplet roll off, the sliding angle, to be lower than 10°. [1-3] These two requirements are often considered analogous to each other and therefore both not studied. The interest in superrepellent surfaces has been growing continuously during the last decade. [4-6] This is mainly due to the tremendous potential that superomniphobic surfaces hold for i.a. microfluidic [7], antifouling [8,9], self-cleaning [1,9], filtration [10,11], drag reduction [1,12], chemical shielding [13], droplet manipulation [14] and corrosion protection [15] applications.

The basic principles governing the spreading of a liquid droplet on a surface were discovered by Young, Wenzel, Cassie and Baxter [1,16,17]. They found two possible wetting states to exist for the droplet: the Wenzel state and the Cassie-Baxter state. The latter of the two describes a superrellent surface, and the equation governing the degree of wetting is called Cassie-Baxter equation, written as follows:

$$\cos\theta^* = f_{SL}\cos\theta + f_{SL} - 1, \quad (1)$$

where θ^* is the apparent contact angle, θ is the equilibrium contact angle and f_{SL} is the area fraction of the solid-liquid interface compared to the whole surface area shadowed by the droplet. Roughness of the surface affects the area fraction term, and θ contains the effect of the surface material. Equation 1 can often be used in explaining changes in wettability. [13,18,19]

Superrepellency is most often achieved with a so-called hierarchical surface structure that consists of a nanostructure on top of a microstructure and is combined with surface modification that lowers the surface energy. With careful enough manipulation of the surface asperities, it is possible to reach even an extremely strong superomniphobicity without paying too much attention to the surface chemistry [6], but practical reasons usually limit the extent to which this can be accomplished.

A multitude of different techniques have been utilized in fabricating hierarchical surface structures [20-24], but the used materials always limit the possible fabrication methods. For hard and resistant substrate materials, like stainless steel, modification of the surface structure is often very difficult or even impossible, in which case a coating might be required. [25] The vast number of applications, containing stainless steel surfaces, that could benefit from superomniphobicity, makes studying the matter meaningful. Some papers have been published presenting superomniphobic coatings on steel surface, but the coatings were mainly quite thick and had plenty of room for improvement in performance and durability. Also, only few of them used stainless steel as a substrate. [26-28] Slippery liquid-infused porous surfaces (SLIPS) have also been used to achieve strongly omniphobic coatings on steel. [29]

A common problem with nanocoatings is their poor mechanical stability, and finding new solutions to reinforce them is a challenging task. One possibility to tackle this problem is by using layered structures that have not been very extensively studied regarding superomniphobic coatings. The main challenge is to strengthen the nanoparticle layer without suppressing the functionality it produces. Atomic layer deposition (ALD) has earlier been shown to enhance the mechanical durability of nanoparticle films and nanocolloidal crystals. [30-32] It was therefore chosen for this study as the method for nanoparticle layer reinforcement.

The goal of this study was to produce a new kind of superomniphobic coating on stainless steel, exploiting a layered nanostructure. Superoleophobic surfaces have been made using nanoparticles synthesized by flame spray pyrolysis, and combined with a top layer of a fluorosilane. [33] However, the herein used combination of the three chosen fabrication methods has not been studied before, to the extent of our knowledge. We were striving for a very thin coating with strong repellency against various liquids. Even though the coating method is applied to stainless steel in this study, a variety of substrate materials could be chosen. In general, LFS offers an economically efficient, well scalable and flexible way to fabricate nanomaterials. Figure 1 describes schematically the stepwise fabrication process of the coating.

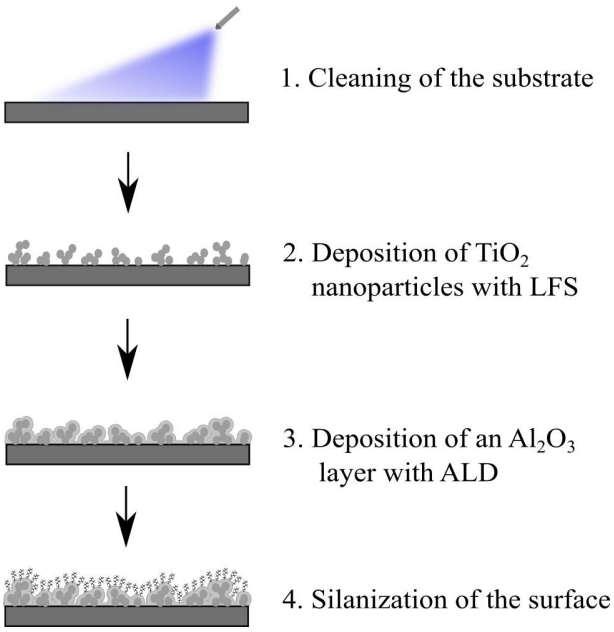

Figure 1. The entire fabrication process of the coating presented schematically in steps.

The process can be divided into four distinct steps. First, the steel substrate was cleaned with various solvents. Secondly, TiO_2 nanoparticles were deposited on the substrate via liquid flame spray (LFS) to provide a suitable surface topography. Thirdly, the nanoparticle layer was coated with a thin Al_2O_3 layer using ALD, in order to reinforce the deposited nanoparticle layer, and

lastly the surface was covered with fluorosilane molecules for lowering the surface energy. The used coating materials were mainly chosen due to experimental experience, assisting in controlling their synthesis processes and the end product. All the steps along with the characterization methods are described in more detail in the following section.

EXPERIMENTAL SECTION

Materials

Austenitic stainless steel plates (ø 17 cm, thickness of 0.6 mm) were acquired from Fiskars Finland Oy Ab and cleaned with acetone (99.5+ %, VWR International), isopropanol (IPA, 99.8 %, VWR International) and deionized (DI) water prior to the actual coating process. The samples were dried with a lint-free cloth and pressurized air. TiO_2 nanoparticles were synthesized from titanium(IV) isopropoxide (TTIP, 97+ %, Alfa Aesar) dissolved in IPA. The precursors for ALD process were trimethylaluminum (TMA, Volatec Oy) and water. (Heptadecafluoro-1,1,2,2-tetrahydrodecyl) trichlorosilane (HDF, 97+ %, Gelest) dissolved in hexane (95%, Sigma-Aldrich) was used for silanization. Test liquids for contact and sliding angle measurements were DI water, diiodomethane (DIM, 99 %, Sigma-Aldrich), ethylene glycol (EG, 99.8 %, Sigma-Aldrich), commercial olive oil (OO) and hexadecane (HDEC, 99 %, Sigma-Aldrich). The set of test liquids were selected primarily on the basis of their surface tension. The surface tension values in 20°C for DI water, DIM, EG, OO and HDEC are 71.99 (25°C) [34], 50.88 (20°C) [35], 47.99 (25°C) [34], 32.0 (20°C) [36] and 27.49 (20°C) [35] mN/m, respectively.

Liquid Flame Spray

LFS is an aerosol synthesis method for producing a variety of metal and metal oxide nanoparticles and –coatings. It can be classified as a specific type of flame spray pyrolysis method, and several publications have been written describing the synthesis process in detail. [37-42] However, there are no earlier publications with the experimental setup used in this paper. The setup consisted of a burner, a so-called residence tube and the substrate that is to be coated, as presented in figure 2.

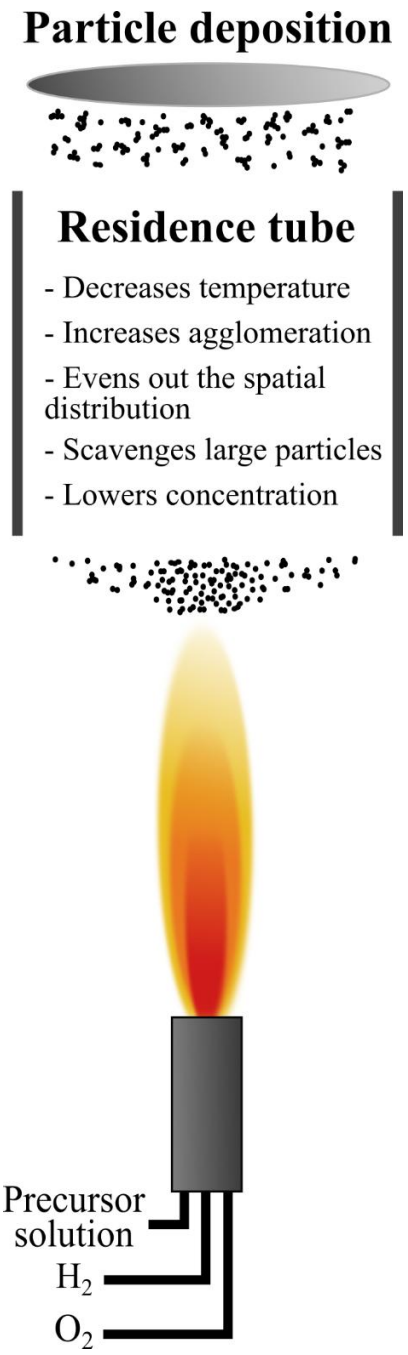

Figure 2. A schematic representation of the LFS coating setup with the description of the effect of the residence tube.

In LFS synthesis, a liquid precursor solution is fed to a burner along with hydrogen and oxygen flows. The hydrogen flow atomizes the liquid jet and also acts as a combustion gas. The atomized droplets go through a complex combination of mechanisms in the flame, including

precursor decomposition and particle nucleation, resulting in nanoparticle formation. In this study, a precursor solution with metallic Ti concentration of 50 mg/ml was fed to the flame with a feed rate of 12 ml/min, and the used hydrogen and oxygen flows were set to 50 and 15 l/min, respectively.

What distinguishes the rest of the process in this study from a more conventional LFS synthesis, is the addition of a residence tube between the burner and the substrate. It modifies the particle flow emerging from the flame and lowers the temperature on the substrate. Maximum temperatures of about 2600°C have been measured close to the burner [38], whereas the temperatures measured after the residence tube have ranged from around 200 to 500°C. The residence tube promotes agglomeration and leads to some particle losses to the walls, but also scavenges large particles and evens out the spatial distribution, which should help in producing a uniform coating across the substrate area. [43,44] In the particle deposition, the substrate was placed on the end of the residence tube for a specific coating time, chosen to be 6 s for the final coating.

Atomic Layer Deposition

ALD is a specific type of chemical vapor deposition method, where the substrate is exposed to isolated gas pulses in a cyclic manner. ALD can be used to coat objects of practically all geometries, and the resulting layer is extremely even and conformal. One of the most common industrial branches utilizing the method nowadays is electronics, but the method has also proven to be suitable for producing different kinds of passivation and protective layers. [46,47]

Here, the LFS-coated samples were first oxidized with mixtures of oxygen (grade 5) and nitrogen flows at 300°C. First, a mixture with approximately 12 % of oxygen was used for 15

min, after which the oxygen fraction was raised to 36 % for 1 min. The specific parameter values were arbitrarily selected, ensuring sufficient oxidation of all organic contaminants on the surface. An Al_2O_3 layer with a thickness of 10 nm was then deposited on top of the nanoparticle layer, also at 300°C. The whole process was performed with a Picosun P-1000 ALD system.

Silanization

Liquid phase deposition (LPD) of the HDF silane was performed on the ALD-coated samples. Freshly prepared samples were silanized in the as-received state. For the samples that had to be stored for an extended time period, a 30 min UV light treatment was applied before the silanization process. This was done in order to decrease the amount of organic impurities that readily accumulate on surfaces during storage in atmospheric conditions, thereby promoting the adherence of silane molecules on the topmost Al_2O_3 layer. UV-C lamps with the peak intensity at 254 nm wavelength were chosen, because they have been observed to decompose organic material without the presence of an additional photocatalyst.

HDF was dispersed into hexane at a ratio of 1:1000 and stirred for 10 min, after which the samples were immersed in the solution for 10 minutes. Subsequently, they were rinsed with hexane and DI water, followed by drying with a nitrogen flow. Details of a successful silanization process are described elsewhere. [47,48]

Surface Properties Analysis

The wettability of the surface was studied using contact angle measurements and sliding angle testing. 4-6 µl droplets of test liquids were placed on the surface and filmed at the same time. The static contact angles were determined, when the shape of the droplet had stabilized, and the

accuracy of the measurement was estimated to be around ± 1°. Sliding angles were tested on a tilted surface by adjusting the inclination angle to a certain value, placing a liquid droplet on the surface and observing if it rolls off or sticks to it.

Microscratch testing was performed mainly to assess the adhesion of the coating to the substrate. The method is typically used for evaluating cohesion and adhesion of thin films and coatings. [49] The testing was based on a Rockwell diamond stylus (diameter of 20 μm and cone angle of 120°) sliding on the coated surface with a continuously increasing load (0.03 to 1 N). The reported load values (or pressure values derived from them) were averaged over three scratches. Friction force, penetration depth and acoustic emission were also measured during the scratching procedure.

Surface Characterization

A Zeiss UltraPlus field emission scanning electron microscope (FESEM) was used for imaging the surface after every fabrication step and after microscratch testing. Cross-sectional milling with Ga^+ ions and SEM imaging was performed with a Zeiss Crossbeam 540 focused ion beam scanning electron microscope (FIB-SEM). In this study, a gold layer was sputtered on the surface for improving electrical conductivity, and a Pt layer on top of that to ensure the protection of the coating during the milling process. The used FIB-SEM was equipped with an energy-dispersive x-ray spectroscopy (EDS) detector, so also elemental mapping was conducted across the produced coating layer alongside cross-sectional imaging.

X-ray photoelectron spectroscopy (XPS) was utilized for analyzing the elemental composition of the surface between the coating steps. The XPS measurements were conducted with non-monochromatic Al Kα radiation ($h\nu$ = 1486.6 eV), and the spectra were recorded in a fixed

analyzer transmission (FAT) mode at normal emission and 20.0 eV pass energy. The binding energy was calibrated to 285.0 eV for aliphatic carbon, and the photoelectron peaks were fitted with a combination of Gaussian and Lorentzian line shapes and Shirley background, using CasaXPS software version 2.3.16. [50]

RESULTS AND DISCUSSION

Determination of parameters and superomniphobicity

The amount of LFS-generated TiO_2 nanoparticles and the thickness of the ALD coating were iterated on the basis of crude mechanical stability testing (observing the effect of the insertion and subsequent removal of a scotch tape with FESEM) and contact angle measurements. Common problems with porous nanoparticle layers are the weak cohesion between the particles and their poor adhesion to the substrate. The goal of the iteration was to find a balance between liquid-repellency and particle layer stability, having emphasis on the repellency. Too short an LFS coating time led to a fairly robust coating, but to an inadequate surface roughness for producing effective repellency. With a long coating time, good repellency could be achieved, but the resulting coating was very fragile and unstable, meaning most of the material came off in the scotch tape test. 6 s was determined suitable. In addition to these problems, too short a coating time led to a net-like microscale structure with a larger aggregate/agglomerate size, and thus lowered the number concentration of secondary particles on the surface. This possibly resulted from some surface treatment done to the steel substrate during its manufacturing process. Once the coating time was increased, the net-like structure got buried under the additional particles, thus increasing the surface coverage of the bare steel significantly.

The role of the ALD layer was to attach the particles more strongly to the substrate and to each other, but without covering the favorable topography and porosity produced by them. Similar effect has earlier been observed in case of solar cells, where the ALD coating increased the mechanical stability of the nanoparticle layer, but lowered its porosity. [51] The first priority in determining the ALD coating thickness was achieving strong omniphobicity. The effect of the ALD coating thickness to the contact angle was studied for the chosen LFS coating time (6 s), and figure 3 describes the contact angle as a function of the thickness along with the measured SA values for the 10 nm ALD thickness are reported for each test liquid. The sliding angle value for hexadecane was not measured, since olive oil with higher surface tension did not fulfill the SA requirement for superrepellency. All of the measured samples were silanized.

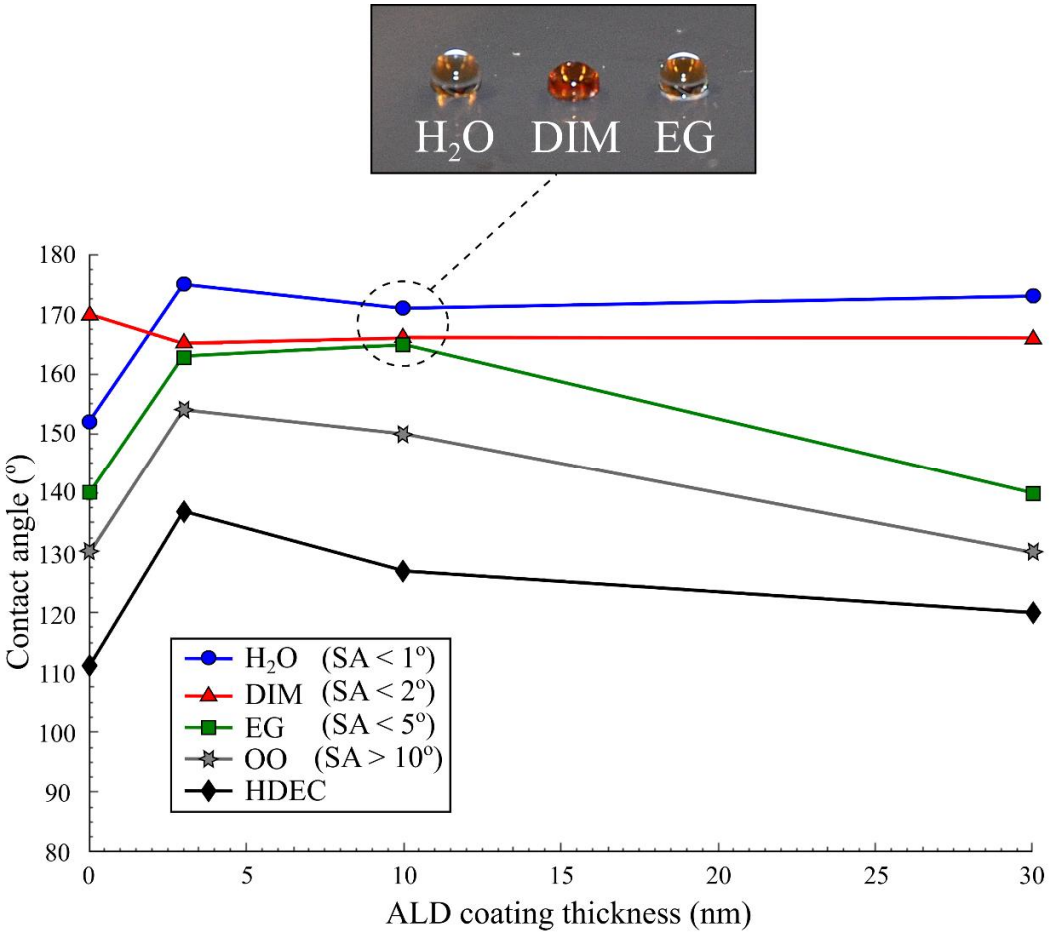

Figure 3. Contact angle as a function of ALD coating thickness for different test liquids. Sliding angle (SA) values are presented in the legend for each liquid, corresponding the ALD thickness of 10 nm. The photo above, presenting droplets of three liquids lying on the surface, was not taken from a CA measurement.

The 3 nm Al_2O_3 layer raised the contact angle in most cases compared to the samples with no ALD coating. This behaviour implies that Al_2O_3 might be a more favourable substrate for LPD of HDF silane than stainless steel or TiO_2, which led to a higher-quality silane layer, indicated by the greater contact angle values. Since a large part of the surface was not covered with nanoparticles after only LFS coating, most of the silane molecules probably adsorbed on the steel surface. Stainless steel is generally a difficult substrate material to silanize without pretreatment. [52] Another possible explanation for this difference could be the stabilizing effect of the ALD layer. If the LFS particle layer without ALD was too unstable, the silanization process might

have rendered the surface structure more unfavourable for omniphobicity by raising the fraction of the solid-liquid interface. Based on equation 1, this would reduce the contact angles. The one measurement point (0 nm for DIM) that is deviating from the trend can be considered a measurement error or an anomaly.

As the ALD coating thickness was increased from 3 nm, the contact angle values began to decrease continuously. This was presumably caused by the Al_2O_3 covering the surface nanostructures that were formed by the nanoparticles. When additional material was deposited on top of the very porous structure, the pores started to fill up, lowering the porosity and the specific surface area. According to the theoretical formulations, this should reduce the apparent contact angles by increasing the solid-liquid area fraction. Simultaneously, the mechanical durability increased (observed earlier with the scotch tape tests), so some kind of a compromise between liquid repellency and durability has to be made, when optimizing the parameters with a certain application in mind. This study does not cover the fine tuning of the parameters from the perspective of mechanical stability, nor are we trying to find optimal parameters for a specific application.

The difference in repellency between the 3- and 10-nm-samples was not too great, so 10 nm was chosen over 3 nm as the more optimal thickness in complete performance of the coating. On the other hand, 30 nm ALD layer already had a reasonably large negative impact on the repellency, at least on the liquids with lower surface tension, so it was discarded as the final coating thickness. If repellency towards high-surface tension liquids would suffice, a thicker ALD layer would likely be a better option.

As already was stated in the introduction section, perfect superomniphobicity is practically impossible to reach. However, our coating fared quite well amongst other reported superomniphobic coatings. Reaching contact angles of over 150° for DI water, diiodomethane, ethylene glycol and olive oil, and with significantly lower sliding angle values than 10° for the first three, we can regard our final coating superomniphobic to a certain extent.

Surface topography after different steps

Imaging of the surface after each coating step gives an insight into the actual role of the different layers. The LFS nanoparticle layer was supposed to be responsible for producing a surface structure that is essential for effective omniphobicity. The ALD layer should work as a stabilizing layer on top of the particle layer without covering the topography. The function of silanization was to lower the surface energy, and it was assumed not to affect the surface structure to a large degree. Figure 4 shows FESEM images after each fabrication step with the chosen parameters. Samples were cut from random locations of the sample plates.

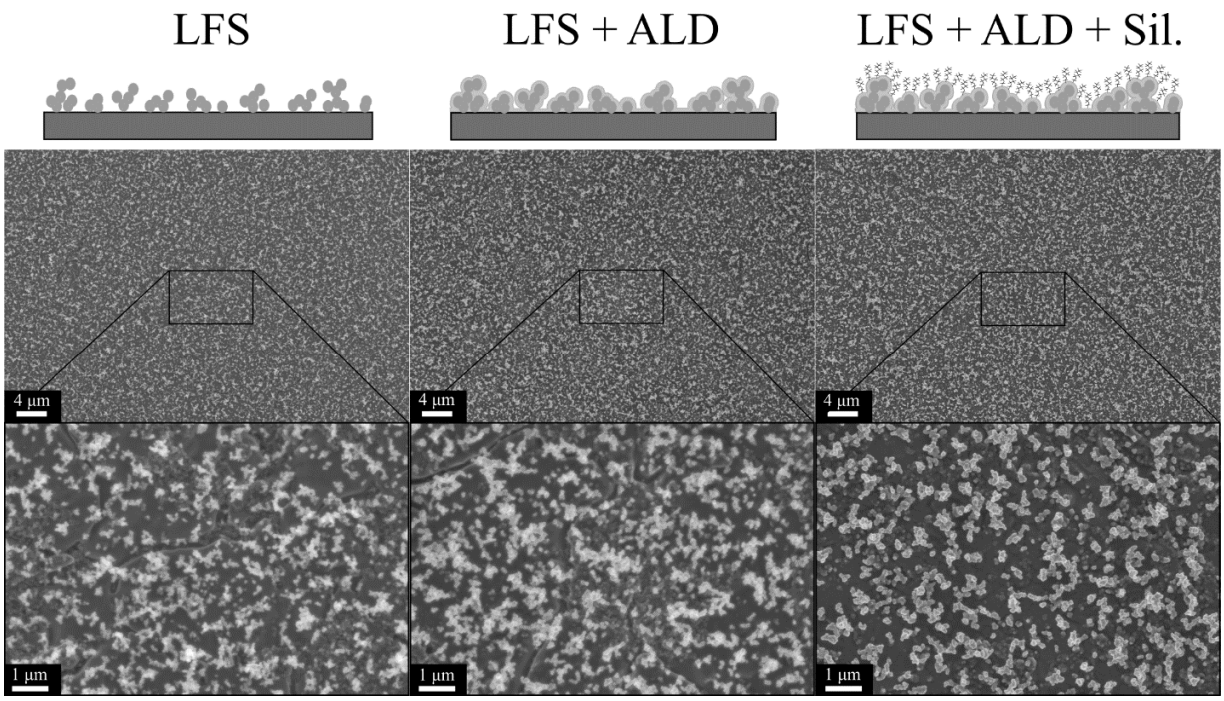

Figure 4. FESEM images of the sample surfaces after every step in the fabrication process. The LFS coating time was 6 s and the ALD coating thickness 10 nm.

The deposited nanoparticles were dispersed very uniformly across the whole imaged area of the samples, and everything from single primary particles to about micron-sized agglomerates in length are observed. Quite a significant portion of the steel surface still remained uncovered. The surface coverage can be estimated, based on graphical analysis (ImageJ) from different FESEM images using automatic thresholding, to be around 30 %. Manual thresholding led to a bit higher percentage of surface coverage, but the user bias is also difficult to quantify in this case. In this sense, automatic thresholding can be seen as the more reliable approximation. This value applies approximately for the samples representing all different steps.

An accurate value is, however, difficult to obtain due to differences in contrast between the FESEM images. Also, a little bit of an oxide particle (probably mostly iron oxide) structure was observed forming on top of the steel surface during the oxidation process before ALD coating.

The oxide particles were of roughly similar size as the titanium dioxide primary particles, which makes distinguishing the real background from the actual coating material more challenging. The precise effect of the oxide structure to the coating properties is unknown, but for example, in case of depositing a similar ALD layer on top of MoS_2, oxidizing the surface in advance was observed to improve the quality of the forming ALD layer. [53]

The visual difference that the thin ALD coating caused to the LFS-coated surface is reasonably small. The primary particle size seems to be roughly 50 nm (considering some nanometers from sample carbonization) and the Al_2O_3 coating increased it slightly. Otherwise, the ALD process did not significantly affect the surface topography, as was expected. Also, the silanization process did not drastically modify the surface structure of the coating. Even though slight discrepancies can be seen between the images representing different steps (figure 4), it has to be accounted for that they are not images of the same sample after each fabrication step, but rather just representing a set of parameters. Some larger differences were observed in case of certain samples (possibly damaged), but Figure 3 can be considered to represent the process fairly well.

Surface elemental analysis by XPS

Based on the FESEM images, the surface structure does not undergo drastic changes during the hierarchical sample fabrication process, but the XPS results reveal that each coating step alters the surface chemistry significantly. The survey spectra and the relative elemental surface concentrations, calculated from the high-resolution spectra, are presented in figure 5.

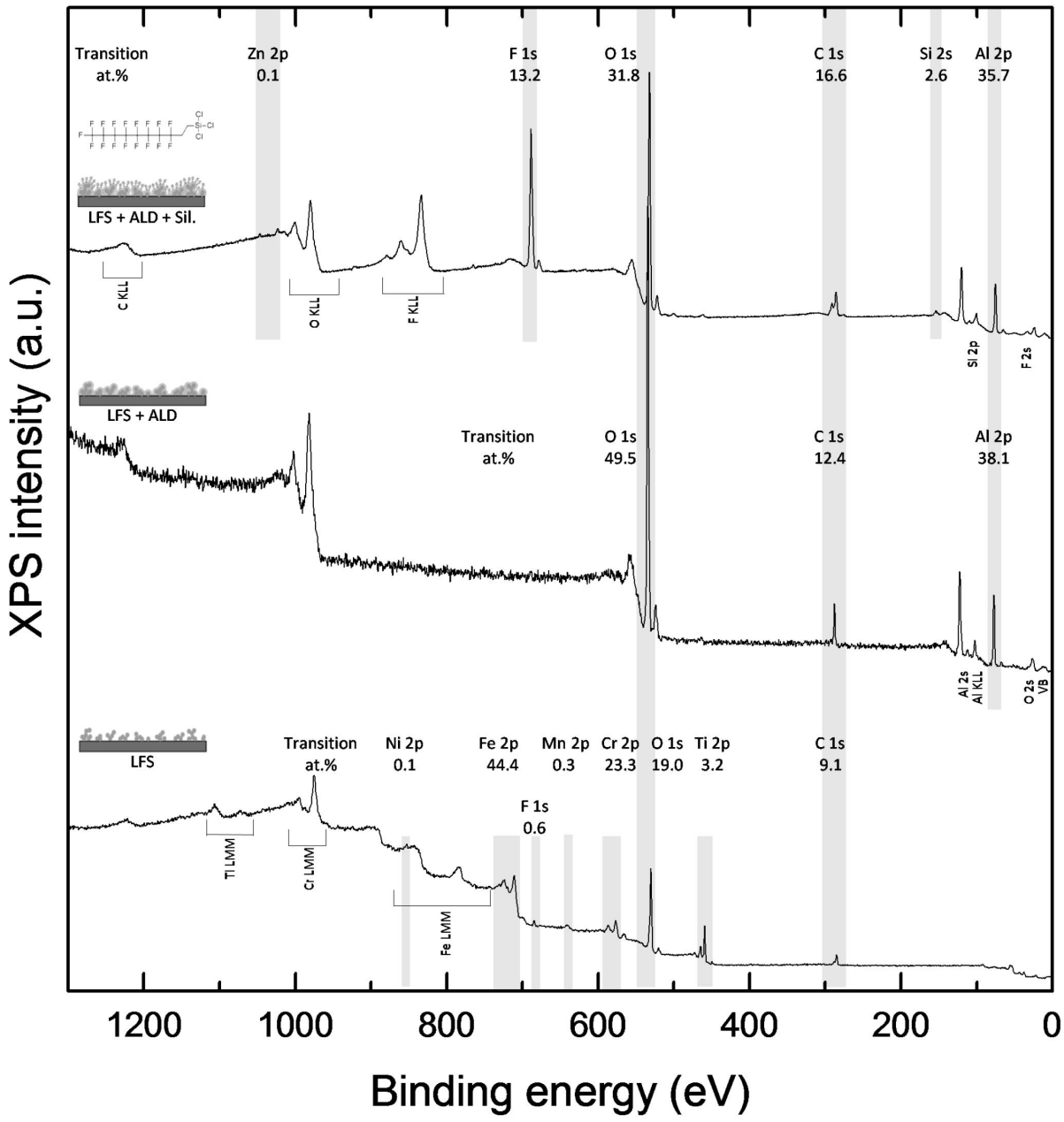

Figure 5. XPS survey spectra and the relative elemental surface concentrations of the samples after each fabrication step.

The survey spectrum of the LFS sample (after the first coating step) shows that the outermost surface (up to ~10 nm information depth) consisted of both TiO_2 nanoparticles and stainless steel. XPS measurements from small areas at different locations reveal that there are local

differences in the Fe concentration. This is in good accordance with the FESEM images (figure 4) that display only a partial surface coverage of the steel surface. Apart from a typical amount of organic contamination and a trace amount of fluorine, the surface was free of impurities. This implies that no additional contamination was produced in the flame, which is usually the case in a normal high-velocity and –temperature LFS process. The organic contaminants originated from the exposure to atmospheric conditions and consist mostly of C-C, C-O and C=O bonds observed in both C 1s and O 1s spectra. The relatively high Fe/Ti atomic ratio (even regarding the low surface coverage) can be attributed to the different information depths of Ti 2p and Fe 2p transitions (~6 nm and 4.5 nm, respectively). For Ti, this discrepancy leads to a larger information volume with a lower relative atomic fraction than for Fe.

The assumption that was made earlier about the evenness and the conformity of the ALD coating, are strongly supported by the XPS measurements after the second fabrication step. The only observed signals came from the Al_2O_3 layer and surface impurities, and no Fe or Ti could be detected. Since the ALD layer thickness (10 nm) was very close to the XPS information depth, the coating material had to be very uniform to attenuate the signal from the nanoparticles completely. The contaminants originated again from the atmospheric exposure during the time between the ALD coating and the XPS measurement.

The survey spectrum of the final multilayered coating (LFS + ALD + Sil.) shows the nanomolecular nature of the HDF silanization process. Signals were observed from both the silane molecules (CF_2 and CF_3 bonds observed in C 1s and F 1s spectra, and Si as a new element on the surface) and the underlying Al_2O_3 layer. The presence of strong Al signal verifies that the HDF (molecular length of 1-2 nm) overlayer is of nanomolecular nature. As there was no Cl visible in the XPS spectrum, it can be assumed that the hydrolysis of the silane molecules

proceeded sufficiently to form a network of covalent bonds with the Al_2O_3 substrate. The presence of chlorine would have implied that some of the molecules were completely, or at least partially, unhydrolyzed, which typically leads to a chemically less robust topmost layer. The uniform coverage of silane molecules throughout the sample was confirmed by inspecting high-resolution F 1s spectra from several small (~10 μm) detection areas. The analysis of the high-resolution C 1s spectrum reveals a contribution from the organic impurities, in addition to the CF_2 chain, to the C 1s intensity. A trace amount of Zn was also observed, probably caused by the coating cycles of ZnO that were done with the ALD system before the coating of the measured samples. This is, nevertheless, insignificant considering the final coating.

Cross-sectional imaging

Cross-sectional imaging was performed to study the thickness and the topographical features in more detail, and with the EDS analysis we wanted to study the distribution of the Al_2O_3 in the coating. A gold layer was sputtered on top of the sample to enhance electrical conductivity. Also, a layer of platinum had to be deposited on top of the coating to ensure that the true structure was being imaged. Both of these pretreatments are visible in figure 6 that presents cross-sectional SEM images with two different magnifications.

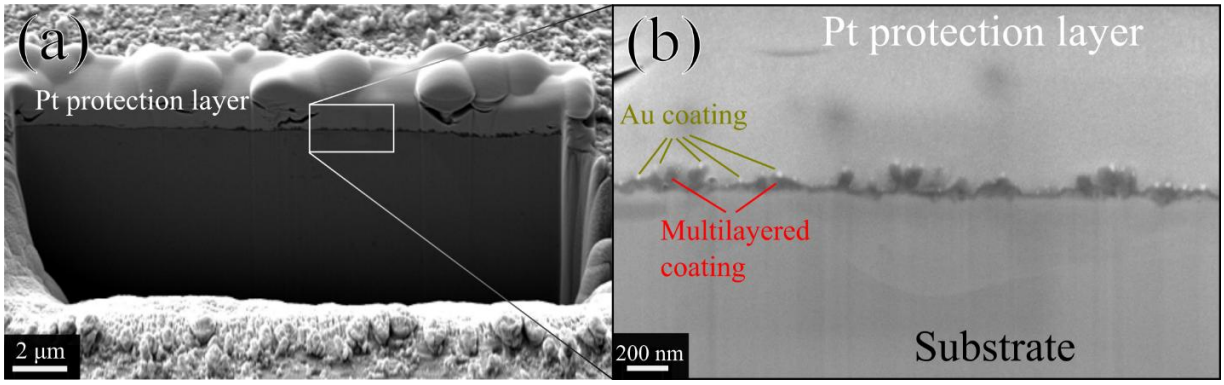

Figure 6. SEM images of (a) the hole milled with FIB using Ga^+ ions and (b) the coating cross section. Different parts of the sample are marked with text.

The small bright dots, visible in figure 6(b), are Au particles originating from the sputtering, and the Pt layer, well visible in figure 6(a), has a thickness of about 1-2 µm. From a larger perspective, the coating seems quite even across the sample area, but the higher magnification reveals the undulating surface topography produced by the nanoparticle agglomerates. The thickness of the coating varies generally between minimum value of ca. 10-15 nm, probably corresponding to areas with only ALD and silane layers, and the maximum value of about 160-200 nm (a wide estimation due to uncertainties), based on the SEM images. If we approximate the area of the coating in the images graphically, and calculate the thickness of a hypothetical, completely even layer with the same cross-sectional area, we get an average value of around 70 nm. This is in no sense an accurate measure and it varies roughly ± 10 nm between different images, but it gives an idea of the size scale.

Since the resolution of the SEM images is not adequate to make accurate approximations, the EDS results can be used to support the observed thickness values. They showed an Al Kα signal coming from the entire length of the cross section that has been interpreted as the coating thickness from the SEM images. This also supports the hypothesis that the ALD layer covers the titania agglomerates across the whole particle layer, and penetrates deep into the porous layer.

This transport inside the layer is probably essential for the reinforcing function of the ALD coating. Considering both the calculated average value and the estimated maximum thickness of around 180 nm, the produced coating is the thinnest reported superomniphobic coating, as far as we know. However, the deposition of the platinum layer might densify some of the larger agglomerates, thus compressing the layer a little. The EDS measurement showed an Al Kα signal coming from the entire length of the cross section, which supports the hypothesis that the ALD layer covers the titania agglomerates across the whole particle layer, and penetrates deep into the porous layer. This transport inside the layer is probably essential for the reinforcing function of the ALD coating.

Microscratch testing

The microscratch testing was performed to assess the adhesion of the coating to the substrate and its performance under load. Figure 7 presents optical and FESEM images of one of the scratches produced on the surface. The discrepancies between different scratches were quite minor, so one scratch represents all of them very well. The pressure values were calculated by dividing the normal force pushing down the diamond tip by half of the area of the circle (20 μm in diameter) projected by the tip on the sample surface. Therefore, in every case the pressure values are approximations based on averaging over the entire scratch width, as they are presented to give an impression of the order of magnitude. Only about a half of the circle area contribute to the real pressure values, since rear half of the moving tip does not come in contact with the surface. The lowest reported pressure value is definitely lower than the actual average value, because the whole tip area has not come in contact with the surface due to low penetration, thus underestimating the average pressure.

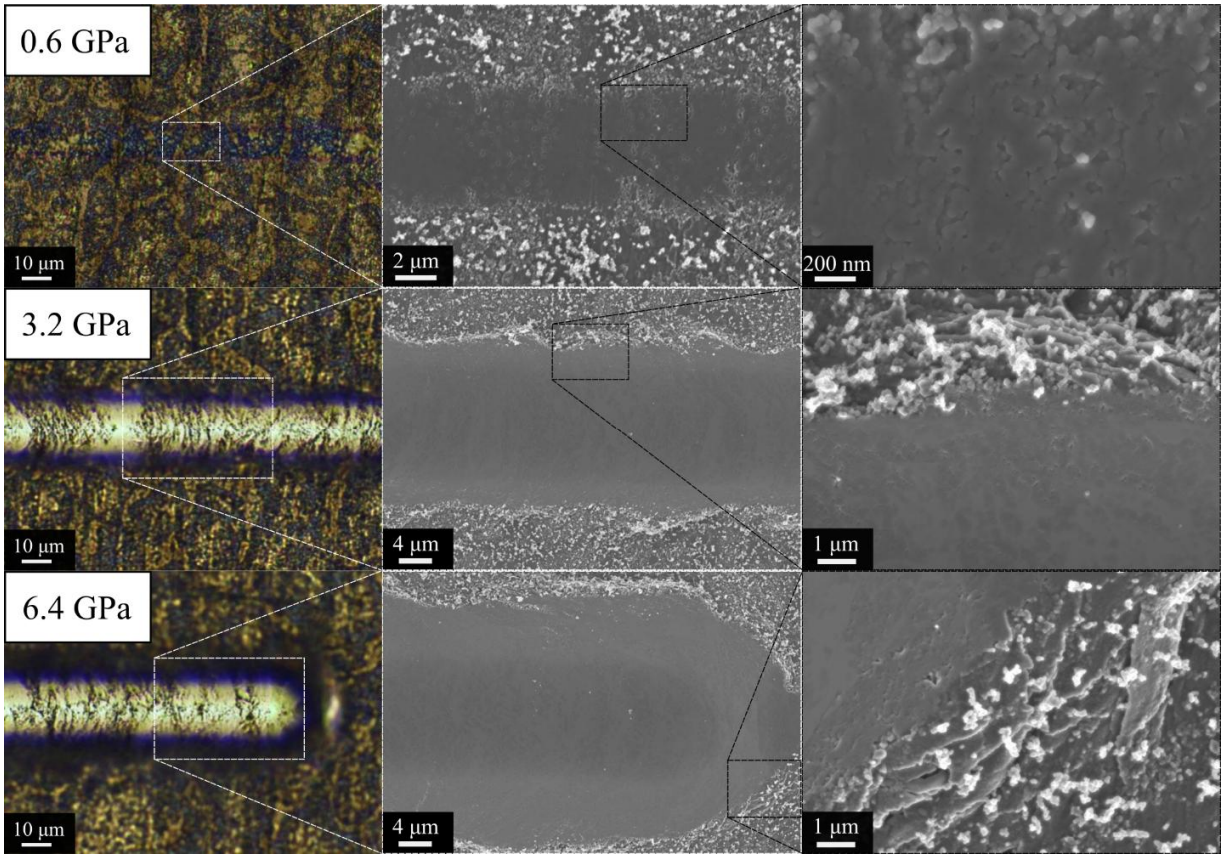

Figure 7. Optical and FESEM images of the scratch made in microscratch testing. The pressure values were calculated by dividing the normal force with the projected area of the diamond tip. The contact pressures refer to normal loads of 0.1, 0.5 and 1 N.

Already with the lowest pressures, a clear scratch groove formed. In the groove, the surface smoothened and the roughness was lost, which is generally detrimental for effective omniphobicity. This implies that the coating is not especially durable against mechanical pressing or abrasion. However, it seems that the coating material is not really detaching from the substrate, but rather just flattening under pressure. The FESEM images with highest magnifications show the squashed nanoparticle agglomerates on the track of the diamond tip. Based on this observation, the adhesion of the particles to the substrate can be considered fairly good. The mechanical stability could possibly be enhanced by promoting the interparticle

cohesion or by choosing a harder nanoparticle material. However, the latter option could further weaken the layer, if the cohesion between the particles in the agglomerates is lowered.

As the normal force was increased, the bottom of the scratch smoothed down further and the substrate material started piling up on the edges. Deducing from the lower pressure parts of the scratch, the particles formed a very thin layer on the bottom of the scratch. The pile-up did not seem to affect the coating topography on the edges significantly, but mostly just shape the underlying substrate. Since the coating is extremely thin, no cracking or delamination occured, which can also be a sign of the particle agglomerates not being very strongly interconnected to each other, but rather just attached to the substrate. In a way, this fullfills the goal, because we were attempting to minimize the amount of material used in producing the favourable surface structure and chemistry. All in all, the surface topography that is necessary for an efficient omniphobicity is lost too easily for the coating to be suitable for applications experiencing moderate to high wear. If weaker repellency would be adequate, the thicker ALD layer could help with this problem.

The measurements performed during the scratching did not reveal anything very surprising. There was no acoustic emission throughout the scratching process, and the coating had no notable effect on the penetration depth of 5 μm into the stainless steel substrate. The measured friction coefficient, reaching the end value of 0.35, seemed to oscillate a little in the beginning, possibly due to the coating topography and reorganizing of its surface structure, but this should have no significant effect on any properties we were interested in regarding this study.

CONCLUSIONS

We fabricated a new type of a superomniphobic coating on stainless steel, consisting of three nanolayers. First, a TiO_2 nanoparticle layer was deposited on a cleaned steel substrate by liquid flame spray with a residence tube added to the experimental setup. The nanoparticle layer was then reinforced with a thin layer of Al_2O_3 produced with atomic layer deposition, and the surface was lastly covered with fluorosilane molecules in a liquid phase deposition process. The topographical and chemical structures were characterized with SEM and XPS methods. The analyses showed that underlying nanoparticles determined the physical surface structure, whereas the silanization dominated the surface chemistry. The ALD process produced an extremely uniform and conformal 10-nm-thick middle layer, thus having no significant impact on the surface structure. Based on the literature we found on the subject, the multilayered coating was thinner than any superomniphobic coating reported so far, with a calculated average thickness of about 70 nm. The final coating expressed strong omniphobicity, forming contact angles greater than 150° for deionized water, diiodomethane, ethylene glycol and olive oil, with sliding angles below 5° for the first three of the mentioned test liquids. The adhesion between the coating material and the substrate seemed reasonably good based on microsratch testing, but the surface structure could not stand much pressure without losing the roughness that is essential for an effective omniphobicity.

If this combination of methods were to be used for a practical application, the parameters would have to be tuned for the specific application, while making a compromise between the repellency and the mechanical stability. This is caused by the effect of ALD thickness on both of these properties. Producing a thicker layer of Al_2O_3 enhances the durability of the coating, simultaneously weakening the repellency. In the future, combinations of other materials utilizing a similar structure could be also studied.

ACKNOWLEDGEMENTS

The work was performed within the DIMECC HYBRIDS (Hybrid Materials) programme. We want to acknowledge the financial support from the Finnish Funding Agency for Innovation (Tekes, grant number 1236/13) and all of the participating companies. We are grateful to Fiskars Finland Oy Ab for providing the stainless steel substrates used in this study. We would also like to thank Prof. Minnamari Vippola from Materials Science at TUT for interpreting some of the results. Janne Haapanen acknowledges financial support from Academy of Finland, project "Nanostructured large-area antibacterial surfaces (nLABS, grant no 278 846)".

REFERENCES

(1) Bhushan, B.; Jung, Y., C. Natural and biomimetic artificial surfaces for superhydrophobicity, self-cleaning, low adhesion, and drag reduction. *Prog. Mater. Sci.* **2011,** *56*, 1-108.

(2) Sun, T.; Feng, L.; Gao, X.; Jiang, L. Bioinspired Surfaces with special wettability. *Acc. Chem. Res.* **2005,** *38*, 644-652.

(3) Antonini, C.; Villa, F.; Bernagozzi, I., Amirfazli, A.; Marengo, M. Drop Rebound after Impact: The Role of the Receding Contact Angle. *Langmuir* **2013,** *29*, 16045-16050.

(4) Ellinas, K.; Tserepi, A.; Gogolides, E. From Superamphiphobic to Amphiphilic Polymeric Surfaces with Ordered Hierarchical Roughness Fabricated with Colloidal Lithography and Plasma Nanotexturing. *Langmuir* **2011,** *27*, 3960-3969.

(5) Tuteja, A.; Choi, W.; Mabry, J.M.; Mckinley, G.H.; Cohen, R.E. Robust omniphobic surfaces. *PNAS* **2008,** *105 (47)*, 18200-18205.

(6) Liu, T.; Kim, C.-J. Turning a surface superrepellent even to completely wetting liquids. *Science* **2014,** *346 (6213)*, 1096-1100.

(7) Lai, Y.-K.; Tang, Y.-X.; Huang, J.-Y.; Pan, F.; Chen. F.; Zhang, K.-Q.; Fuchs, H.; Chi, L.-F. Bioinspired TiO_2 Nanostructure Films with Special Wettability and Adhesion for Droplets Manipulation and Patterning. *Sci. Rep*. **2013,** *3 (3009)*.

(8) Genzer, J.; Efimenko, K. Recent developments in superhydrophobic surfaces and their relevance to marine fouling: a review. *Biofouling* **2006,** *22 (5)*, 339-360.

(9) Brown, P.S.; Bhushan, B. Mechanically durable, superomniphobic coatings prepared by layer-by-layer technique for self-cleaning and anti-smudge. *J. Colloid. Interf. Sci.* **2015,** *456*, 210-218.

(10) Ge, D.; Yang, L.; Wang, C.; Lee, E.; Zhang, Y.; Yang, S. A multi-functional oil-water separator from a selectively pre-wetted superamphiphobic paper. *Chem. Commun.* **2015,** *51*, 6149-6152.

(11) Wang, N.; Zhu, Z.; Sheng, J.; Al-Deyab, S.S.; Yu, J.; Ding, B. Superamphiphobic nanofibrous membranes for effective filtration of fine particles. *J. Colloid. Interf. Sci.* **2014,** *428*, 41-48.

(12) Lee, C.; Kim, C.-J. Underwater Restoration and Retention of Gases on Superhydrophobic Surfaces for Drag Reduction. *Phys. Rev. Lett.* **2011,** *106 (014502)*.

(13) Vahabi, H.; Wang, W.; Movafaghi, S.; Kota, A.K. Free-Standing, Flexible, Superomniphobic Films. *ACS Appl. Mater. Interfaces* **2016,** *8*, 21962-21967.

(14) Vahabi, H.; Wang, W.; Davies, S.; Mabry, J.M.; Kota, A.K. Coalescence-Induced Self-Propulsion of Droplets on Superomniphobic Surfaces. *ACS Appl. Mater. Interfaces* **2017,** *9*, 29328-29336.

(15) Jin, C.; Li, J.; Han, S.; Wang, J.; Sun, Q. A durable, superhydrophobic, superoleophobic, and corrosion-resistant coating with rose-like ZnO nanoflowers on a bamboo surface. *Appl. Surf. Sci.* **2014,** *320*, 322-327.

(16) Wenzel, R.N. Resistance of solid surfaces to wetting by water. *Ind. Eng. Chem.* **1936,** *28*, 988-994.

(17) Cassie, A.B.D.; Baxter, S. Wettability of porous surfaces. *Trans. Faraday Soc.* **1944,** *40*, 546-551.

(18) Wang, W.; Salazar, J.; Vahabi, H.; Joshi-Imre, A.; Voit, W.E.; Kota, A.K. Metamorphic Superomniphobic Surfaces. *Adv. Mater.* **2017,** *29*, 1700295.

(19) Vahabi, H.; Wang, W.; Popat, K.C.; Kwon, G.; Holland, T.B.; Kota, A.K. Metallic superhydrophobic surfaces via thermal sensitization. *Appl. Phys. Lett.* **2017,** *110*, 251602.

(20) Ganesh, V.A.; Dinachali, S.S.; Nair,A.S.; Ramakrishna, S. Robust Superamphiphobic Film from Electrospun TiO_2 Nanostructures. *ACS Appl. Mater. Interfaces* **2013,** *5*, 1527-1532.

(21) Jiang, D.; Fan, P.; Gong, D.; Long, J.; Zhang, H.; Zhong, M. High-temperature imprinting and superhydrophobicity of micro/nano surface structures on metals using molds fabricated by ultrafast laser ablation. *J. Mater. Process. Tech.* **2016,** *236*, 56-63

(22) Kumar, R.T.R.; Mogensen, K.B.; Bøggild, P. Simple Approach to Superamphiphobic Overhanging Silicon Nanostructures. *J. Phys. Chem. C* **2010,** *114*, 2936-2940.

(23) Li, H.; Yu, S. A stable superamphiphobic Zn coating with self-cleaning property on steel surface fabricated via a deposition method. *J. Taiwan Inst. Chem. E* **2016,** *63*, 411-420.

(24) Muthiah, P.; Bhushan, B.; Yun, K.; Kondo, H. Dual-layered-coated mechanically-durable superomniphobic surfaces with anti-smudge properties. *J. Colloid Interf. Sci.* **2013,** *409*, 227-236.

(25) Chen, K.; Wu, Y.; Zhou, S.; Wu, L. Recent Development of Durable and Self-Healing Surfaces with Special Wettability. *Macromol. Rapid Commun.* **2016,** *37*, 463-485.

(26) Motlagh, N.V.; Birjandi, F.C.; Sargolzaei, J.; Shahtahmassebi, N. Durable, superhydrophobic, superoleophobic and corrosion resistant coating on the stainless steel surface using a scalable method. *Appl. Surf. Sci.* **2013,** *283*, 636-647.

(27) Li, H.; Yu, S.; Han, X. Fabrication of CuO hierarchical flower-like structures with biomimetic superamphiphobicm self-cleaning and corrosion resistance properties. *Chem. Eng. J.* **2016,** *283*, 1443-1454.

(28) Li, H.; Yu, S. Facile fabrication of micro-nano-rod structures for inducing a superamphiphobic property on steel surface. *Appl. Phys. A* **2016,** *122 (30).*

(29) Tesler, A.B.; Kim, P.; Kolle, S.; Howell, C.; Ahanotu, O.; Aizenberg, J. Extremely durable biofouling-resistant metallic surfaces based on electrodeposited nanoporous tungstite films on steel. *Nat. Commun*. **2015,** *6*, 8649.

(30) Dafinone, M.I.; Feng, G.; Brugarolas, T.; Tettey, K.E.; Lee, D. Mechanical Reinforcement of Nanoparticle Thin Films Using Atomic Layer Deposition. *ACS Nano* **2011,** *5 (6)*, 5078-5087.

(31) Zhang, L.; Prosser, J.H.; Feng, G.; Lee, D. Mechanical properties of atomic layer deposition-reinforced nanoparticle thin films. *Nanoscale* **2012,** *4*, 6543-6552.

(32) Zhang, D.; Zhang, L.; Lee, D.; Cheng, Z.; Feng, G. Reinforcing nanocolloidal crystals by tuning interparticle bonding via atomic layer deposition. *Acta Mater.* **2015,** *95*, 216-223.

(33) Wong, W.S.Y.; Liu, G.; Nasiri, N.; Hao, C.; Wang, Z.; Tricoli, A. Omnidirectional Self-Assembly of Transparent Superoleophobic Nanotextures. *ACS Nano* **2017,** *11*, 587-596.

(34) Lide, D.R. CRC Handbook of Chemistry and Physics 88th Edition. **2007,** CRC Press, Taylor & Francis Group, Boca Raton, FL, USA.

(35) Körösi, G.; Kováts, E.sz. Density and Surface Tension of 83 Organic Liquids. *J. Chem. Eng*. *Data* **1981,** *26*, 323-332.

(36) Jones, A.Z. Surface Tension – Definition and Experiments. *ThoughtCo* **Mar. 13, 2017,** thoughtco.com/surface-tension-definition-and-experiments-2699204.

(37) Mäkelä, J.M.; Haapanen, J.; Harra, J.; Juuti, P.; Kujanpää, S. Liquid Flame Spray – A Hydrogen-Oxygen Flame Based Method for Nanoparticle Synthesis and Functional Nanocoatings. *KONA Powder Part. J.* **2017,** *34*, 141-154.

(38) Tikkanen, J.; Gross, K.A.; Berndt, C.C.; Pitkänen, V.; Keskinen, J.; Raghu, S.; Rajala, M.; Karthikeyan, J. Characteristics of the liquid flame spray process. *Surf. Coat. Tech.* **1997,** *90*, 210-216.

(39) Mäkelä, J.M.; Keskinen, H.; Forsblom, T.; Keskinen, J. Generation of metal and metal oxide nanoparticles by liquid flame spray process. *J. Mater. Sci.* **2004,** *39*, 2783-2788.

(40) Pitkänen, A.; Mäkelä, J.M.; Nurminen, M.; Oksanen, A.; Janka, K.; Keskinen, J.; Keskinen, H.; Liimatainen, J.K.; Hellstén, S.; Määttä, T. Numerical study of silica particle formation in turbulent H_2/O_2 flame. *IFRF Combust J.* **2005,** *200509.*

(41) Aromaa, M.; Keskinen, H.; Mäkelä, J.M. The effect of process parameters on the Liquid Flame Spray generated titania nanoparticles. *Biomol. Eng.* **2007,** *24*, 543-548.

(42) Keskinen, H.; Aromaa, M.; Heine, M.-C.; Mäkelä, J.M. Size and velocity measurements in sprays and particle producing flame sprays. *Atomization Spray.* **2008,** *18*, 1-26.

(43) Teisala, H.; Tuominen, M.; Aromaa, M.; Mäkelä, J.M.; Stepien, M.; Toivakka, M.; Kuusipalo, J. Development of superhydrophobic coating on paperboard surface using the Liquid Flame Spray. *Surf. Coat. Tech.* **2010,** *205 (2)*, 436-445.

(44) Tuominen, M.; Teisala, H.; Aromaa, M.; Stepien, M.; Mäkelä, J.M.; Saarinen, J.J.; Toivakka, M.; Kuusipalo, J. Creation of superhydrophilic surfaces of paper and board. *J. Adhes. Sci. Technol.* **2014,** *28 (8-9)*, 864-879.

(45) Miikkulainen, V.; Leskelä, M.; Ritala, M.; Puurunen, R. Crystallinity of inorganic films grown by atomic layer deposition: Overview and general trends. *J. Appl. Phys.* **2013,** *113*, 021301.

(46) Elliott, S.D.; Dey, G.; Maimaiti, Y.; Ablat, H.; Filatova, E.A.; Fomengia, G.N. Modeling Mechanism and Growth Reactions for New Nanofabrication Processes by Atomic Layer Deposition. *Adv. Mater.* **2016,** *28*, 5367-5380.

(47) Vuori, L.; Hannula, M.; Lahtonen, K.; Jussila, P.; Ali-Löytty, H.; Hirsimäki, M.; Pärna, R.; Nõmmiste, E.; Valden, M. Controlling the synergetic effects in (3-aminopropyl) trimethoxysilane and (3-mercaptopropyl) trimethoxysilane coadsorption on stainless steel surfaces. *Appl. Surf. Sci.* **2014,** *317*, 856-866.

(48) Vuori, L.; Leppiniemi, J.; Hannula, M.; Lahtonen, K.; Hirsimäki, M.; Nõmmiste, E.; Costelle, L.; Hytönen, V.P.; Valden, M. Biofunctional hybrid materials: bimolecular organosilane monolayers on FeCr alloys. *Nanotechnology* **2014,** *25 (43)*, 435603.

(49) Kilpi, L.; Ylivaara, O.M.E.; Vaajoki, A.; Malm, J.; Sintonen, S.; Tuominen, M.; Puurunen, R.L.; Ronkainen, H. Microscratch testing method for systematic evaluation of the adhesion of atomic layer deposited thin films on silicon. *J. Vac. Sci. Technol. A* **2016,** *34 (1)*, 01A124.

(50) Fairley, N. CasaXPS: Spectrum Processing Software for XPS, AES and SIMS (Version 2.3.16). *Casa Software Ltd. Cheshire SK9 6N, UK* **2009,** *available: http://casaxps.com/*

(51) Mayon, Y.O.; Duong, T.; Nasiri, N.; White, T.P.; Tricoli, A.; Catchpole, K.R. Flame-made ultra-porous TiO_2 layers for perovskite solar cells. *Nanotechnology* **2016,** *27*, 505403.

(52) Jussila, P; Ali-Löytty, H.; Lahtonen, K.; Hirsimäki, M.; Valden, M. Effect of surface hydroxyl concentration and morphology of aminopropylsilane thin films on austenitic stainless steel. *Surf. Interface Anal.* **2010,** *42*, 157-164.

(53) Yang, J.; Kim, S.; Choi,W.; Park, S.H.; Jung, Y.; Cho, M.-H.; Kim, H. Improved Growth Behavior of Atomic-Layer-Deposited High-k Dielectrics on Multilayer MoS_2 by Oxygen Plasma Pretreatment. *Interfaces* **2013,** *5*, 4739-4744.

AUTHOR INFORMATION

Corresponding Author

*E-mail: miika.sorvali@tut.fi

ORCID Miika Sorvali: 0000-0003-2697-4922

Funding Sources

The study was funded by the Finnish Funding Agency for Innovation (Tekes, grant 1236/13). Some of the work hours were funded from a project by Academy of Finland.